

R. Sharman, W. Hall, T. Keller, and J. Wolff
National Center for Atmospheric Research
Boulder, CO 80307

ABSTRACT

The feasibility of using a high resolution numerical simulation model to forecast mountain wave turbulence (MWT) in an operational setting is investigated. The strategy is to use a multi-nested version of the anelastic Clark-Hall simulation model embedded within the Rapid Update Cycle (RUC) operational model domain. The RUC forecast provides the initialization and boundary conditions for the time integration of the Clark-Hall model. The initial evaluation focuses on a commercial airliner MWT encounter near Alamosa, Colorado, which occurred on Feb. 27, 2004. Flight recorder data was available to compare with simulations for this case. Subsequent tests focus on the time period 2-9 Mar 2004 which, according to available pilot reports of turbulence, contained a good mix of turbulent (including severe) and nonturbulent days over the Rockies from New Mexico up through Wyoming (32N-42N). Resolution sensitivities, CPU requirements, and required integration cycles are being evaluated. The goal of this work is to determine whether next generation numerical weather prediction models can be used to directly forecast MWT.

1. INTRODUCTION

Anyone who has flown regularly over large mountain ranges such as the Rocky Mountains knows that turbulence frequently occurs above and to the lee of complex mountainous terrain. However, the problem of forecasting this MWT is particularly difficult. The resolution of operational forecasting models is too coarse to resolve many of the terrain features and smaller scale flow distortions such as breaking waves and wind reversals. In addition, these models often employ the assumption of hydrostatic balance, which excludes the possibility of simulating the intrinsically nonhydrostatic motions often observed in mountain waves.

Outside of the operational setting, researchers have investigated the details of flow over complex terrain using computer intensive high resolution numerical simulations. The explosion of

computing capacity in recent years has made it possible to use high resolution mesoscale models to simulate scales of motion relevant to aircraft turbulence (10m – 1000 m roughly). With multi-nesting capability it is possible to reconstruct within a local region, the meteorological environment surrounding an aircraft turbulence encounter to include large scales of up to one or two thousand km down to scales approaching the size of an aircraft. In fact this technique has been used with some success to recreate actual aircraft turbulence encounters with clear-air turbulence (Clark et al. 2000), convectively-induced turbulence (Lane et al. 2003) and terrain-induced turbulence (Clark et al. 1997). However, until recently the computer resources required for these simulations have prohibited using these high resolution models in an operational setting.

Here we address the feasibility of using the multi-nested Clark-Hall high resolution numerical model used successfully to model mountain waves and turbulence in a research mode (e.g., Clark 1977, Clark and Peltier 1977, Peltier and Clark 1979) to forecast mountain wave turbulence (MWT) in an operational setting. The Clark-Hall model is described in Clark (1977), Clark and Hall (1991), and Clark (1979). NCEP's Rapid Update Cycle (RUC) forecast model (Benjamin et al. 2004), which captures the larger scale weather features, provides the initialization and boundary conditions for the time integration of the Clark-Hall model.

The initial evaluation described here focuses on a commercial airliner turbulence encounter over the Rocky Mountains near Alamosa, Colorado. This case was chosen because actual flight recorder data was available to compare to the model results. Comparing with the flight recorder data eliminates the inherent difficulties involved with turbulence pilot reports (PIREPs), such as inaccuracies in position and turbulence intensity. The simulation results to be presented here indicated the presence of mountain waves and wave breaking in this region, with flow reversal, large vertical velocities and accompanying turbulence. The success of using the high resolution model for this initial case

confirms the validity of this approach. Further tests are ongoing using PIREPs for turbulence observations, for both turbulent and nonturbulent cases.

2. ALAMOSA TURBULENCE EVENT

On February 27, 2004 at 0828 UTC a commercial airliner was flying at FL330 (flight level 33,000 ft MSL, or about 10 km elevation) near Alamosa, Colorado when it encountered sudden, severe turbulence. Prior to the event the flight had been smooth and conditions clear. The pilot reported a 20 kt airspeed indicator deviation and both positive and negative 800ft altitude changes.

Analysis of the on-board aircraft data recorder showed the aircraft cruising straight and level at 33,000 ft moments before the encounter. The turbulence lasted approximately one minute, with positive and negative roll and pitch variations, and vertical accelerations varying between +1.5 g and .07 g within 3 seconds. In addition, during the event the background atmospheric wind speed decreased sharply and the wind direction shifted momentarily from 240° to 160°, resulting in a brief shift from tail wind to cross-wind. The region of intense turbulence was associated with an altitude gain of 800 ft within the first 43 seconds, followed by an altitude loss down to 32,800 ft, then altitude undulations of decreasing magnitude in a very distinct pattern suggestive of a mountain wave. These altitude undulations were accompanied by strong vertical velocity variations. The phase relationship between the altitude and vertical velocity variations was approximately 90 degrees, which is characteristic of atmospheric gravity waves. In addition, the pilot reporting mountain wave activity at the time of the incidence.

Independent confirmation of the presence of gravity waves on the day of the incident is shown in the MODIS satellite water vapor imagery taken approximately 3 hours before the event (Fig. 1). Note the distinct wave pattern in the water vapor signal. This image, provided by Mr. Nathan Uhlenbrock (SSEC/CIMMS at the University of Wisconsin, Madison), was diagnosed to contain waves with a horizontal wavelength of 19-20 km. Accounting for the time difference, this is in rough agreement with the 14 km wavelength derived from the flight recorder data.

Surface maps at 0 and 3 UTC showed a high pressure region near the border of Colorado and New Mexico and a low pressure trough moving into eastern Colorado. This resulted in a pressure gradient perpendicular to the mountain ridges in

southern Colorado. Pressures at surface stations along the Front Range, just east of Rocky Mountains, continued to decrease through 9 UTC. Near flight level, at 250 mb, the wind speeds increased between 0 and 12 UTC. This was associated with the jet stream dropping down from northwestern Colorado into central Colorado (Fig. 2).

RUC model output for this day captured the gross features, including the placement of the jet stream and flow direction over southern Colorado. Fig. 3 shows the flight track superimposed on the 0900 UTC RUC model analysis flow field at 33,000 ft. The red dot indicates the turbulence incident based on the flight recorder data. Note that the flow direction is approximately parallel to the flight track and perpendicular to the mountain ridges in this area. Sounding data derived from the nearest grid point to the incident using the RUC data shows two prominent high wind peaks (Fig. 4). At lower levels the wind speed reaches 33 m/s near 3.0 km, resulting in a very strong wind across the mountain peaks. The upper level wind maximum of 34 m/s occurred at 15 km. Between these two layers the wind speed drops to 17 m/s. A high wind speed near mountain top is frequently associated with the generation of atmospheric gravity waves and turbulence (e.g., Sharman et. al. 2000). In addition, the sharp drop in wind speed above the lower level high velocity layer is conducive to amplification and breakdown of gravity waves (e.g., Smith 1977).

The presence of wave signatures in both the aircraft flight recorder data and the satellite image, combined with atmospheric conditions known to be conducive to mountain wave formation and amplification, suggests the turbulence was likely caused by gravity waves generated by flow over the mountainous topography near Alamosa, CO. Thus this incident is ideal for investigating the utility of the using the Clark-Hall simulation model for forecasting MWT.

3. NUMERICAL MODEL

The high resolution Clark-Hall model used to simulate this MWT event was developed by Drs. Terry Clark and Bill Hall at the National Center for Atmospheric Research (NCAR). This nonlinear, time-dependent numerical model solves the anelastic equations of motion on a terrain-following coordinate system. The model is described in Clark (1977), Clark and Hall (1991), and Clark (1979). This model has been used for high resolution simulation studies of a variety of mesoscale phenomena from large amplitude

mountain lee waves (e.g., Clark and Peltier 1977, Peltier and Clark 1979), thunderstorms (e.g., Clark 1979), gravity waves induced by frontogenesis (Gall et al. 1988), convectively-induced gravity waves (Clark et al. 1986, Hauf and Clark 1989) and terrain-induced turbulence in the lee of Lantau Island in Hong Kong (Clark et al. 1997). Comparisons of Clark-Hall model output to observations have been performed as well. For example in Clark and Gall (1982) this model was particularly successful in reproducing the observed features surrounding mountain wave events, while in Clark et al. (1997), Clark et al. (2000), and Lane et al. (2003) the model was able to reproduce the gross features of observed turbulence events. Thus this model should be a good choice for simulating MWT events. Note, however, that mesoscale models in general cannot be expected to reproduce the exact timing and intensity of observed turbulent patches due to problems associated with such effects as initialization uncertainties and oversimplified sub-grid scale turbulence parameterizations. Nonetheless, as stated, this model has been relatively successful in reproducing the gross aspects of observed turbulent patterns.

For this case the Clark-Hall model was set up and executed using three progressively higher resolution nested domains. The outer domain was initialized using data from the RUC model at 0100 UTC and integrated for two hours of model time before spawning domain 2. Both domains 1 and 2 were then run for another two hours of model time before spawning the innermost highest resolution domain 3. The three domain configuration was integrated in time until 0830 UTC. Time varying lateral boundary conditions derived from time-interpolated 3 hourly RUC data were continuously applied to the outer domain to account for changing synoptic conditions during the several hours of model integration time.

The use of nested domains allows for increasing resolution, down to a horizontal resolution of 1 km in the innermost third domain. The grid size and horizontal resolution for each domain is shown in the table below. An important feature of this model is the ability nest in the vertical as well. Thus vertical grid spacing was variable, with increasing resolution in the nested domains.

domain	grid size (X,Y,Z)	horizontal resolution
1	122x122x45	12 km
2	122x122x72	4 km
3	194x194x72	1 km

A plot of the terrain in domains 1 and 3 is shown in Fig. 5. The location of vertical slices shown in the Figs. below is indicated by the red line in domain 3.

4. NUMERICAL MODEL RESULTS

Results from the third or innermost domain of the high resolution simulation at 0830 UTC showed a large amplitude overturning wave near the incident site with associated regions of reduced wind speed and enhanced vertical velocities. The flow deceleration and wind reversal is evident in a plot of the east-west component (U) of the horizontal wind velocity (Fig. 6) in a vertical slice parallel to the flight track. Here the incident site is marked by the X. Note the patch of zero (white) and negative (green) U velocity just upwind of the incident site, between 10 and 12 km elevation. Color contours of total speed show a significant deceleration of the background flow, from an incoming flow velocity of 30 ms^{-1} down to near 10 ms^{-1} in the wave region.

Vertical velocities along this vertical slice show regions of upward and downward velocities on the downwind side of the mountain peaks (Fig. 7). The region of maximum vertical velocity, indicated in red, occurs at the accident site. A similar region of large upward velocity was probably responsible for the sudden altitude gain experienced by the aircraft at the beginning of the turbulence encounter. The horizontal wavelength of the wave pattern in the simulation varies from about 10 to 20 km, in good agreement with the MODIS satellite image shown in Fig. 1 and the flight data recorded altitude variations. Note that this wavelength is short enough that nonhydrostatic effects are important (e.g., Queney 1948, Sharman and Wurtele 2004), thus emphasizing the necessity of using a high resolution (at least 2-4 km horizontally) nonhydrostatic model to correctly model MWT.

Fig. 8 shows that the eddy diffusion coefficient, KM, which is a measure of the sub-grid scale turbulent kinetic energy (TKE) in this model, also has maximum values in this region. Since the model horizontal resolution here is 1 km, most turbulent motion that would affect aircraft are at these subgrid scales. In order to use this model or a similar model operationally, statistics of the subgrid tke or eddy dissipation rate would have to be output and calibrated against aircraft turbulence encounters, either using flight data recorder information or

automated *in situ* eddy dissipation rate measurements (Cornman et al. 1996).

The horizontal extent of the flow distortions due to the mountain induced wave motion is clearly seen in the X-Y horizontal plots at flight level 330 (10 km). Contours of total speed (Fig. 9) show the aircraft flight track crossing the northern edge of a region of decelerated flow that extends approximately 50 km in X and Y (outlined in blue). Large parts of this region have wind speeds less than 10 m s^{-1} , including a few areas of stagnate flow (in white). Close examination of the flow vectors (Fig. 10) reveals that the wind direction changes from southwesterly to south-southeasterly near the incident site. This is in striking agreement with the variations in wind speed and direction measured by the aircraft's flight data recorder. Note there is a small region south of the incident site, highlighted by the yellow arrow, in which the flow has actually reversed direction. The eddy diffusion coefficient, KM, which is proportional to TKE, shows numerous small patches in the area of decelerated and reversed flow (Fig. 11).

In summary, flow distortions resulting from the breaking mountain waves in the simulation show striking similarities to the measurements from the onboard flight data recorder. In particular, there is good agreement in the location of turbulence, horizontal wind shifts associated with disturbed flow, and regions of high vertical velocity. Thus in this severe turbulence encounter case, the simulation model was able to reproduce the details of the wave/turbulence structures indicated in the flight data recorder.

5. CONCLUSIONS

The numerical simulation of the MWT encounter near Alamosa, CO by a commercial aircraft clearly shows mountain wave activity and associated flow reversals and turbulence over the region in southern Colorado very near the incident site. The close agreement between the numerical simulation and data from the onboard flight data recorder show the feasibility of using high resolution simulations in forecasting mountain wave induced turbulence.

It is important to note that, at least in this particular case, the mountain wave wavelength was relatively short, between 10-20 km, therefore the use of a nonhydrostatic model with at least 2-4 km horizontal resolution is required to correctly model the MWT associated with this event.

It is evident from time sequences of images of

KM (proportional to subgrid TKE) that the wave breaking regions and turbulence are highly transitory, and therefore in an operational setting, some method will need to be developed to account for this variability, perhaps in a probabilistic sense. This will have to be done by comparisons to other cases with flight recorder data or with aircraft containing the automated *in situ* turbulence measurement algorithm.

Further tests are currently being conducted using PIREPs to determine days with and without turbulence over mountainous terrain. Specifically, the focus is on a mix of turbulent (including severe encounters) and nonturbulent days over the Rockies from New Mexico up through Wyoming (32N-42N) during the period 2-9 Mar 2004. Results from these simulations, including resolution sensitivities, CPU requirements, and required integration cycles, will be presented at the conference. These results should help determine whether next generation nonhydrostatic nested numerical weather prediction models such as the Weather Research and Forecast Model (WRF) can be used to directly forecast MWT.

Acknowledgments. This research is in response to requirements and funding by the Federal Aviation Administration (FAA). The views expressed are those of the authors and do not necessarily represent the official policy or position of the FAA.

REFERENCES

- Benjamin, S.G., G.A. Grell, J.M. Brown, T.G. Smirnova, and R. Bleck, 2004: Mesoscale weather prediction with the RUC hybrid isentropic-terrain-following coordinate model. *Mon. Wea. Rev.*, **132**, 473-494.
- Clark, T. L., 1977: A small-scale dynamic model using a terrain-following coordinate system. *J. Comput. Phys.*, **24**, 186-215.
- Clark, T. L. and W. R. Peltier, 1977: On the evolution and stability of finite-amplitude mountain waves. *J. Atmos. Sci.*, **34**, 1715-1730.
- Clark, T. L., 1979: Numerical simulations with a three-dimensional cloud model: Lateral boundary condition experiments and multicellular severe storm simulations. *J. Atmos. Sci.*, **36**, 2191-2215.
- Clark, T. L., and R. Gall, 1982: Three-dimensional numerical model simulations of airflow over mountainous terrain: A comparison with observations. *J. Atmos. Sci.*, **36**, 2191-2215.

- Clark, T. L., T. Hauf, and J. P. Kuettnner, 1986: Convectively forced internal gravity waves: results from two-dimensional numerical experiments. *Quart. J. R. Met. Soc.*, **112**, 899-925.
- Clark, T. L. and W. D. Hall, 1991: Multi-domain simulations of the time-dependent Navier-Stokes equations: Benchmark error analysis of some nesting procedures. *J. Comput. Phys.*, **92**, 456-481.
- Clark, T. L., M. A. Jenkins, J. Coen, and D. Packham, 1996: A coupled atmosphere-fire model: convective feedback on fire-line dynamics. *J. Appl. Meteor.*, **35**, 875-901.
- Clark, T. L., T. Keller, J. Coen, P. Neilley, H.-M. Hsu, and W. D. Hall, 1997: Terrain-induced turbulence over Lantau Island: 7 June 1994 Tropical Storm Russ case study. *J. Atmos. Sci.*, **54**, 1795-1814.
- Clark, T. L., W. D. Hall, R. M. Kerr, D. Middleton, L. Radke, F. M. Ralph, P. J. Nieman, and D. Levinson, 2000: Origins of aircraft-damaging clear-air turbulence during the 9 December 1992 Colorado downslope windstorm: numerical simulations and comparison with observations. *J. Atmos. Sci.*, **57**, 1105-1131.
- Cornman, L. B., C. S. Morse, and G. Cuning, 1995: Real-time estimation of atmospheric turbulence severity from in-situ aircraft measurements. *J. Aircraft*, **32**, 171-177.
- Gall, R., R. T. Williams, and T. L. Clark, 1988: Gravity waves generated during frontogenesis. *J. Atmos. Sci.*, **45**, 2204-2219.
- Hauf, T. and T. L. Clark, 1989: Three-dimensional numerical experiments on convectively forced internal gravity waves. *Quart. J. R. Met. Soc.*, **115**, 309-333.
- Lane, T.P., R.D. Sharman, T.L. Clark, and H.-M. Hsu, 2003: An investigation of turbulence generation mechanisms above deep convection. *J. Atmos. Sci.*, **60**, 1297-1321.
- Peltier, W. R. and T. L. Clark, 1979: The evolution and stability of finite-amplitude mountain waves. Part II: surface wave drag and severe downslope windstorms. *J. Atmos. Sci.*, **36**, 1498-1529.
- Queney, P., 1948: The problem of airflow over mountains. A summary of theoretical studies. *Bull. Amer. Meteor. Soc.*, **29**, 16-26.
- Sharman, R., D. Landau, and M. Wurtele: Another approach to operational forecasting of mountain wave turbulence. Preprints, 38th Aerospace Sciences meeting, American Inst. Aeronautics and Astronautics, Reno, NV.
- Sharman, R. D. and M. G. Wurtele, 2004: Three-dimensional structure of forced gravity waves and lee waves. *J. Atmos. Sci.*, **61**, 664-681.
- Smith, R. B., 1977: The steepening of hydrostatic mountain waves. *J. Atmos. Sci.*, **34**, 1634-1654.

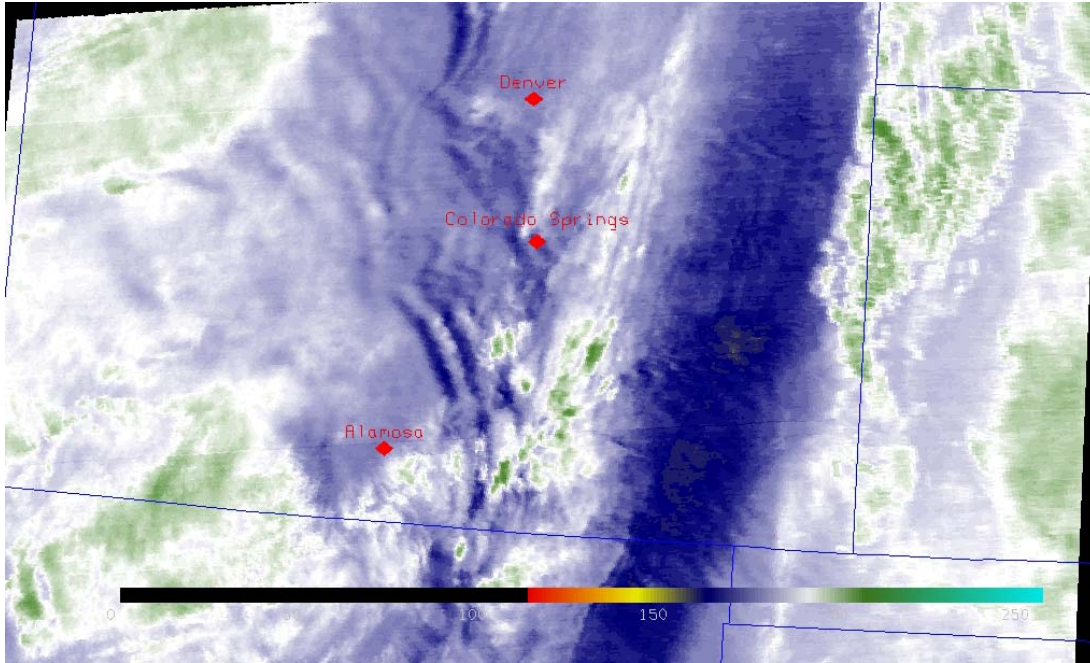


Fig. 1. Water vapor image from MODIS satellite, Feb. 27, 2004 at 0525 UTC. Note the distinct wave pattern northeast of Alamosa, CO.

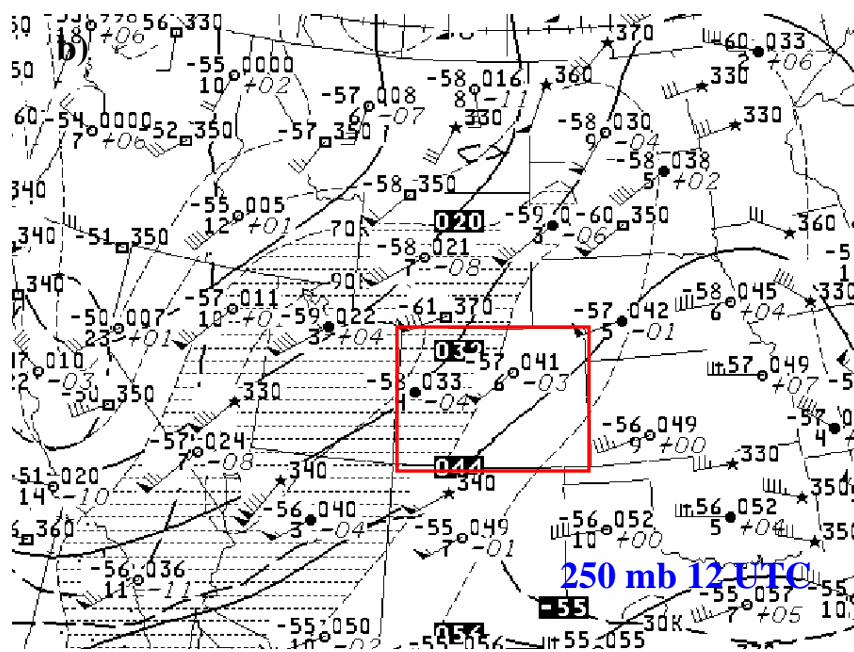
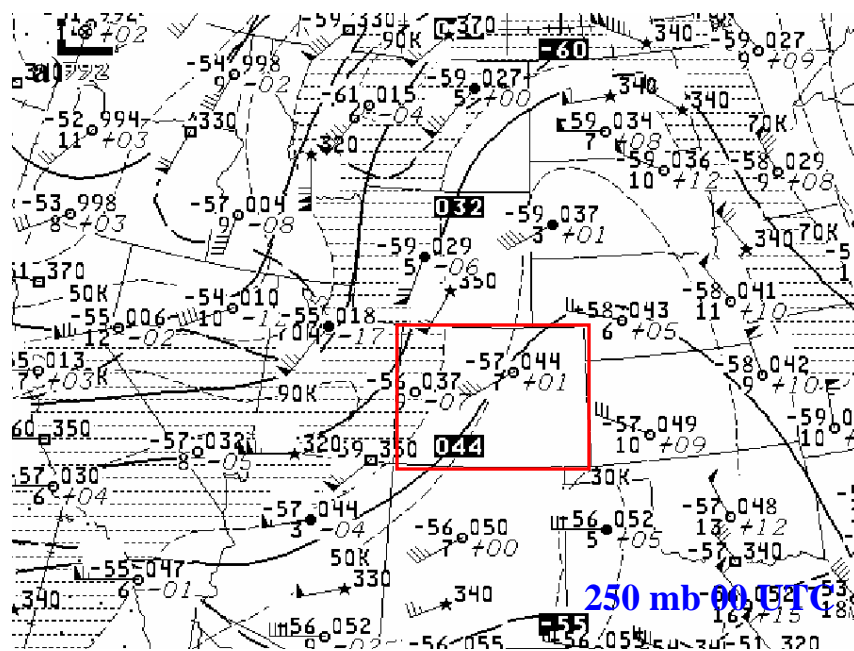


Fig. 2. 250 mb maps for Feb. 27, 2004 at a) 0000 UTC and b) 1200 UTC. The state of Colorado is outlined in red. Note the movement of the jet stream further into western Colorado from 00 to 12 UTC.

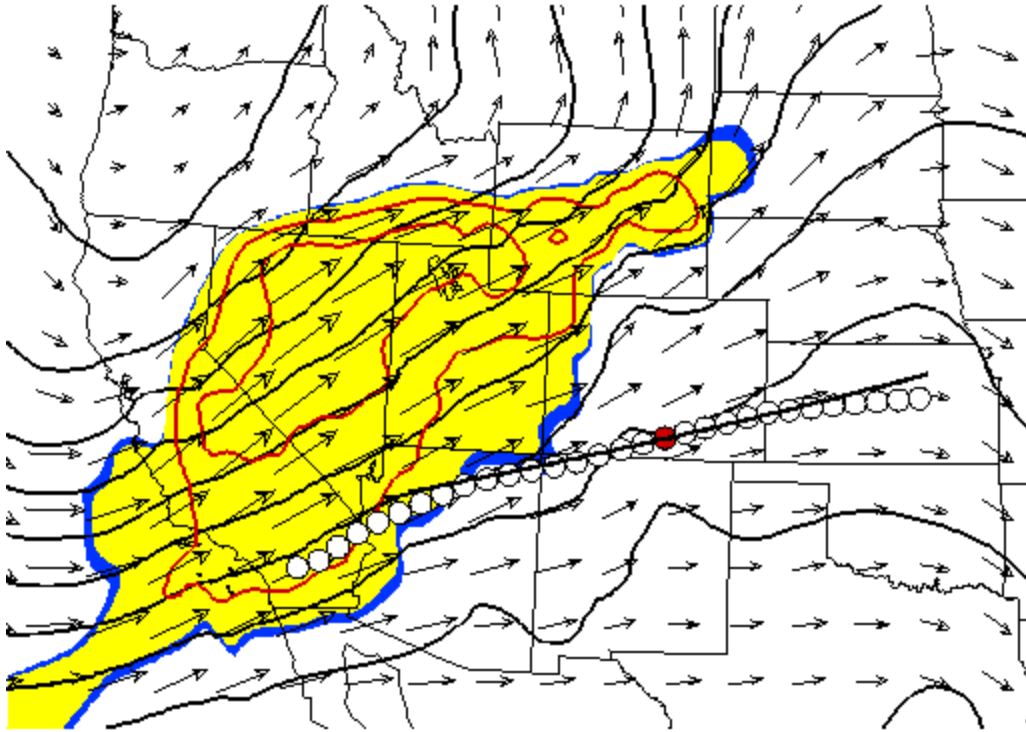


Fig. 3. Wind velocity vectors from the 0900 UTC RUC analysis at FL330 on Feb. 27, 2004. Yellow shading indicates wind speed greater than 36 ms^{-1} . Airline flight track is indicated by open circles. The red filled circle corresponds to the location of intense turbulence from the flight recorder data.

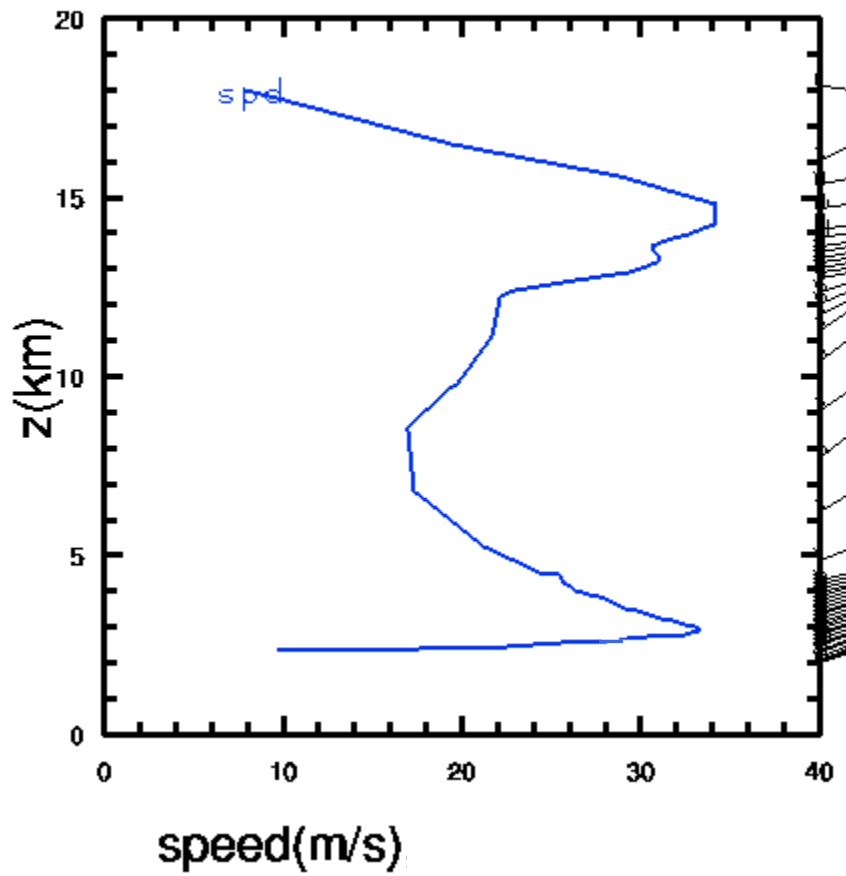


Fig. 4. Vertical distribution of the horizontal wind speed and direction derived from the 0900 UTC RUC model analysis using the nearest grid point to the turbulence encounter as recorded on the flight data recorder.

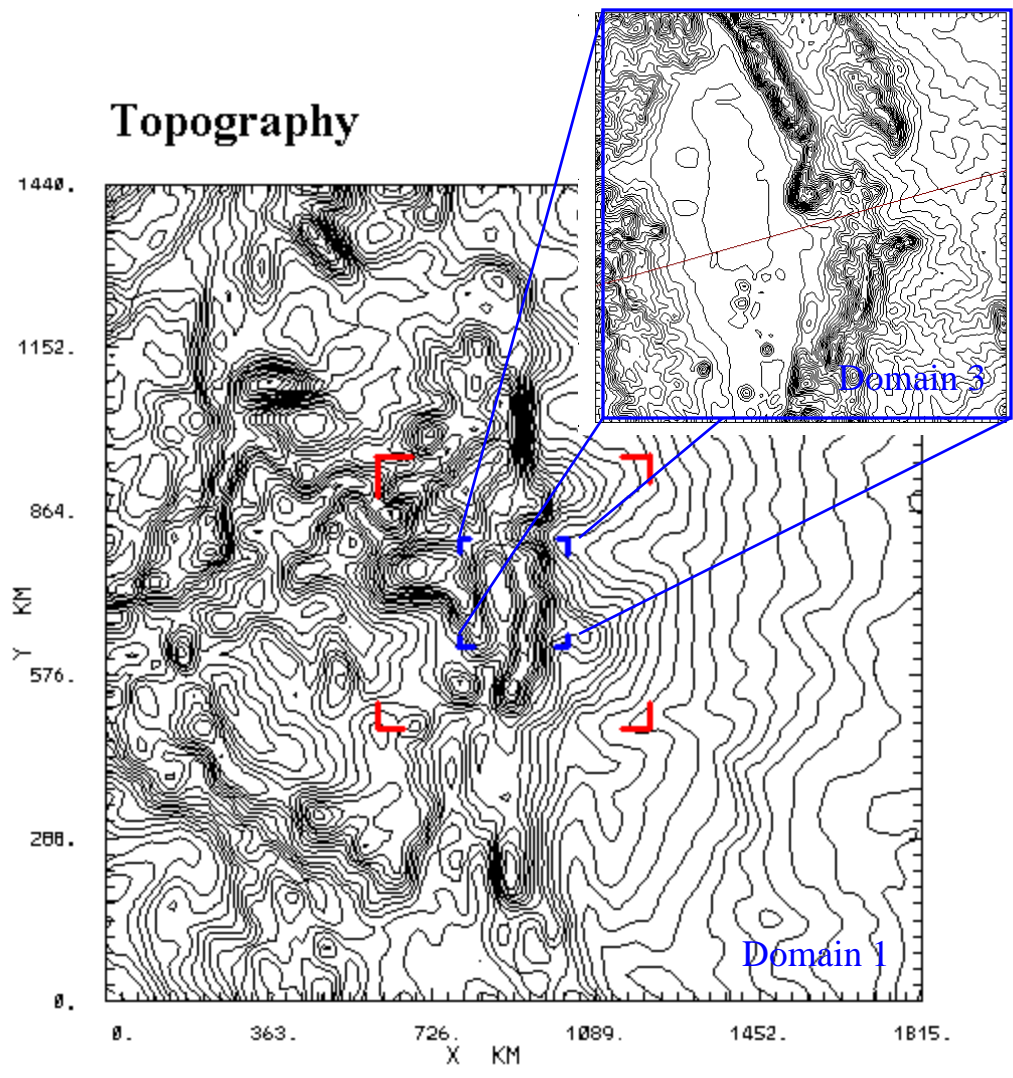


Fig. 5. Terrain contours for the outer domain (domain 1) and inner most domain (domain 3). Red and blue brackets delineate position of domains 2 and 3. Aircraft flight track is represented by red line in domain 3.

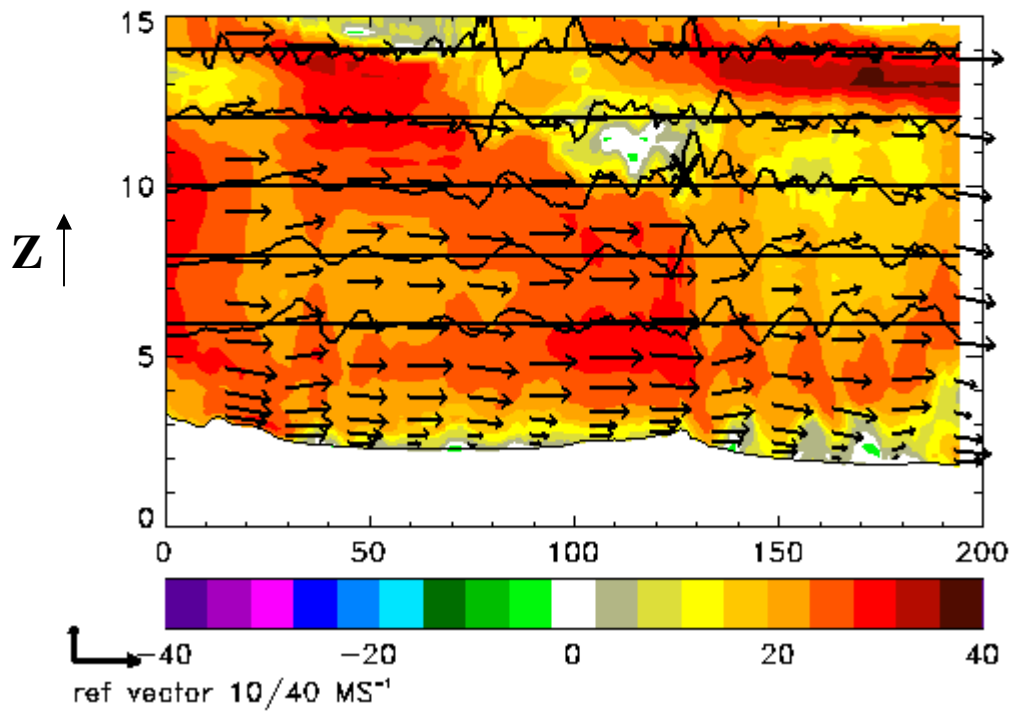


Fig. 6. Color contours of the east-west wind velocity U (m s^{-1}) on a vertical slice along the flight track. Position of the turbulence encounter is marked by the X. Note the region of stagnate (white) and reversed flow (green) just upwind of incident site.

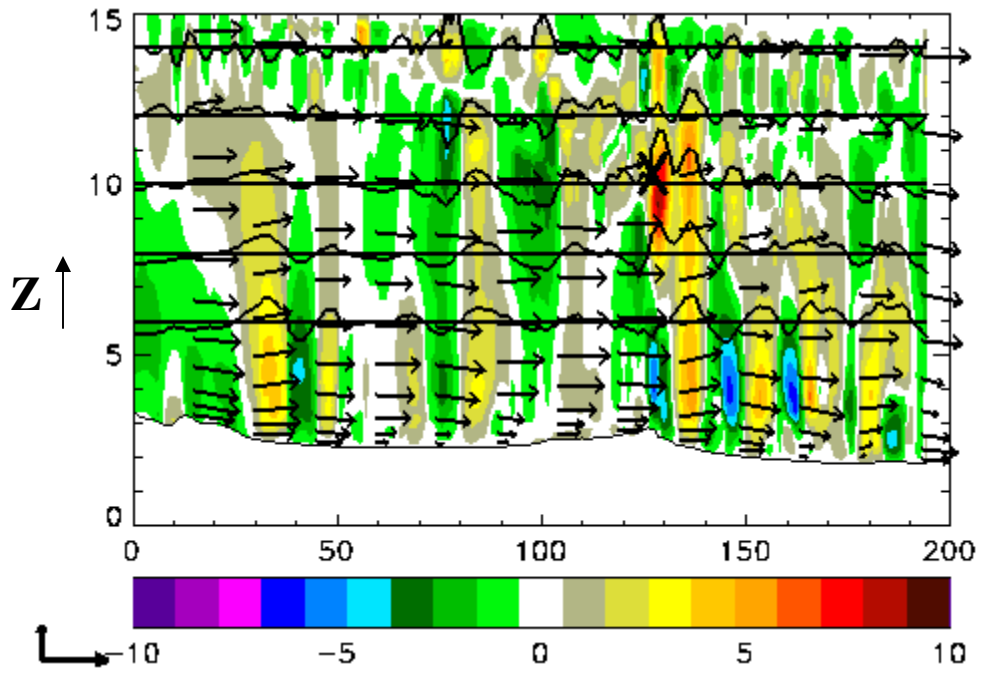


Fig. 7. As in Fig. 6 except color contours of vertical velocity W (m s^{-1}). Note the largest vertical velocity occurs at the incident site marked by the X.

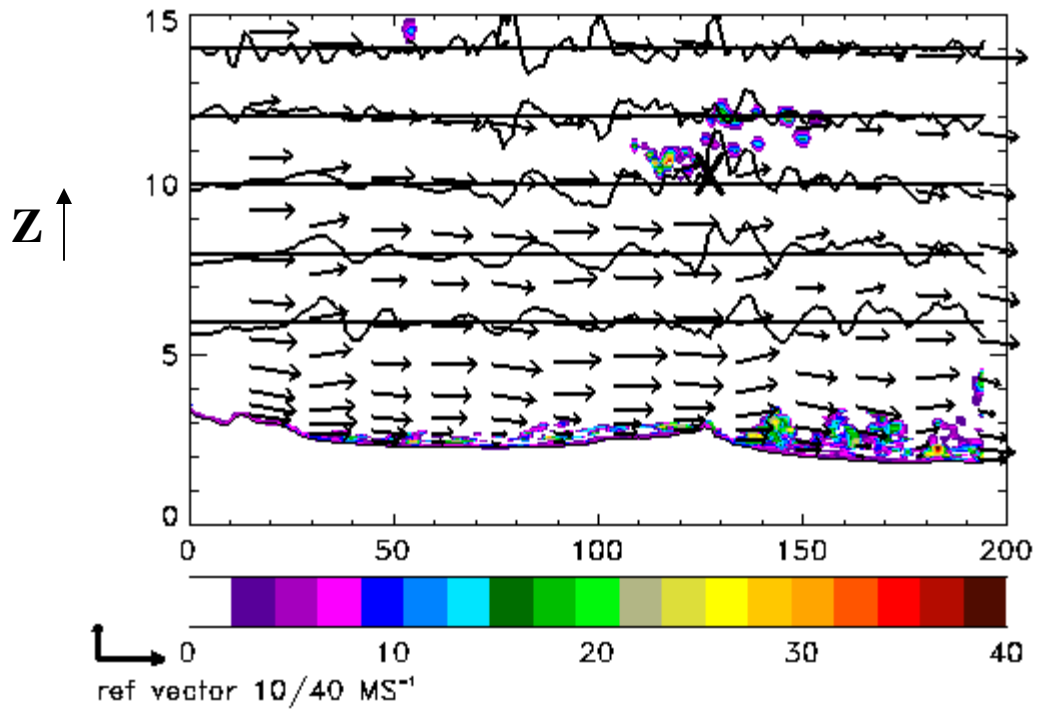


Fig. 8. As in Fig. 6 except color contours of the eddy diffusion coefficient, KM. KM is proportional to sub-grid scale turbulent kinetic energy.

X-Y plot 83000 UTC 10032.8M MSL
SPEED

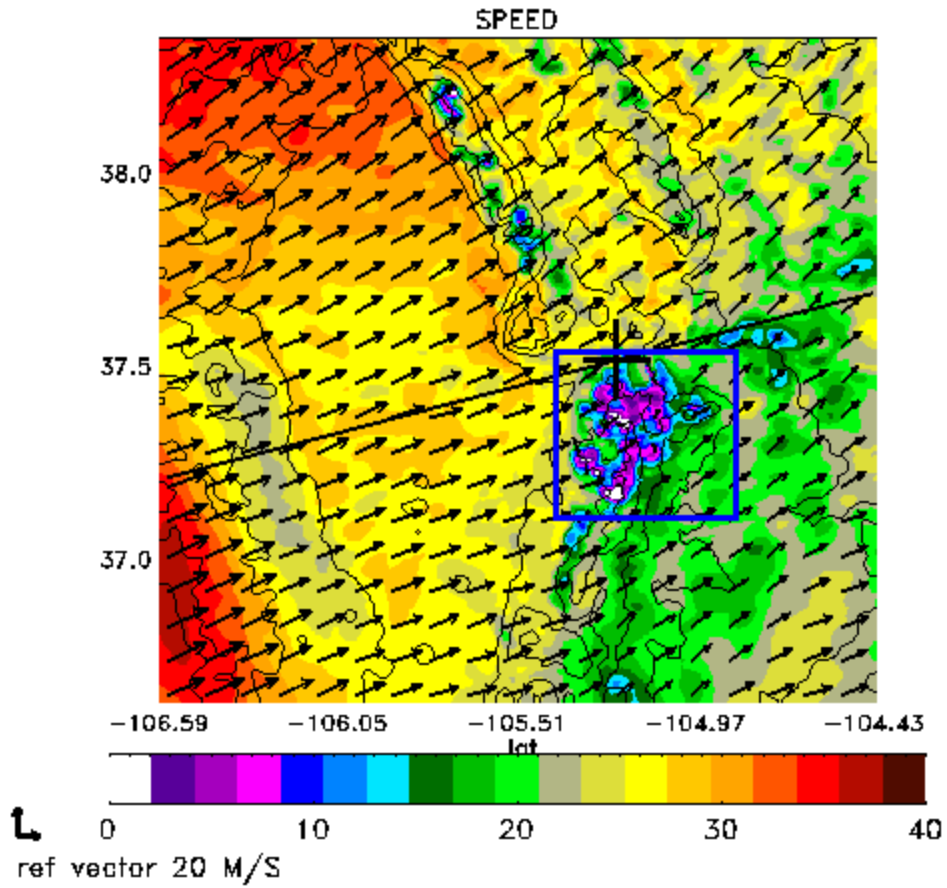


Fig. 9. Color contours of the total horizontal wind speed (m s^{-1}) on an X-Y plane at flight level 330 (10 km). Flight track and incident site are indicated by the black line and + mark. Note the large region of decelerated flow within the blue box.

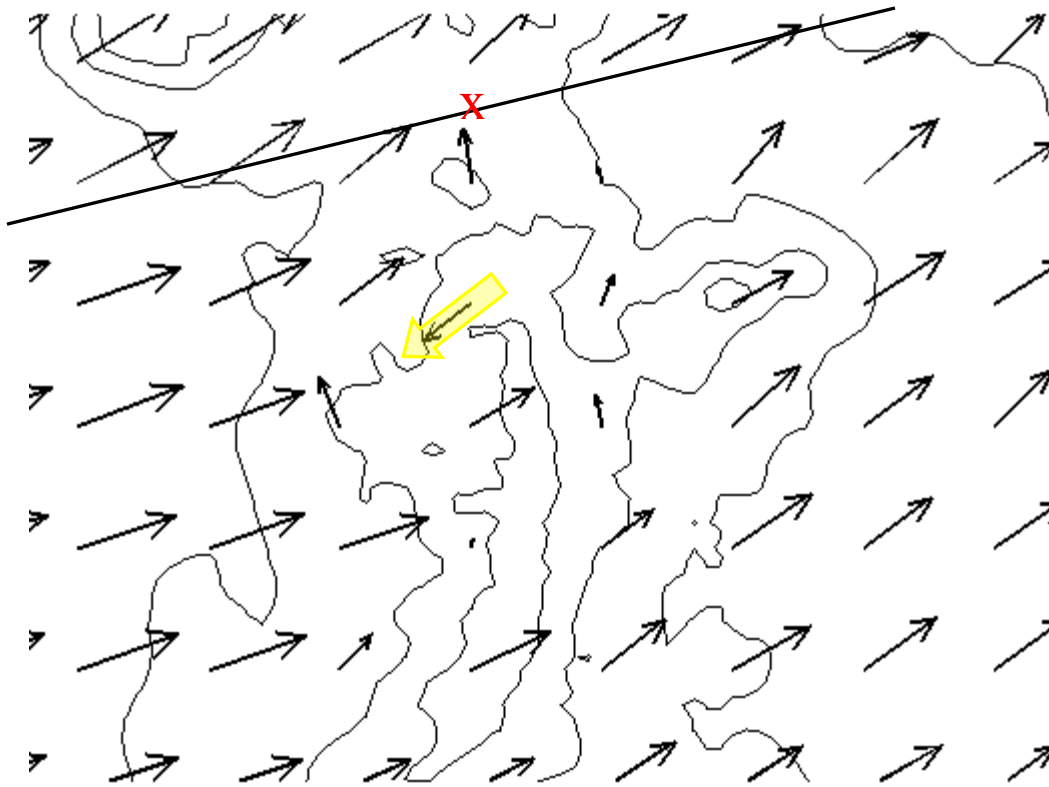


Fig. 10. Plot of the horizontal wind vectors on the X-Y plane at 10 km. Area covered corresponds roughly to the area within the blue box in Fig. 9. Incident site is marked by the red X. Arrow indicating reversed flow is highlighted in yellow.

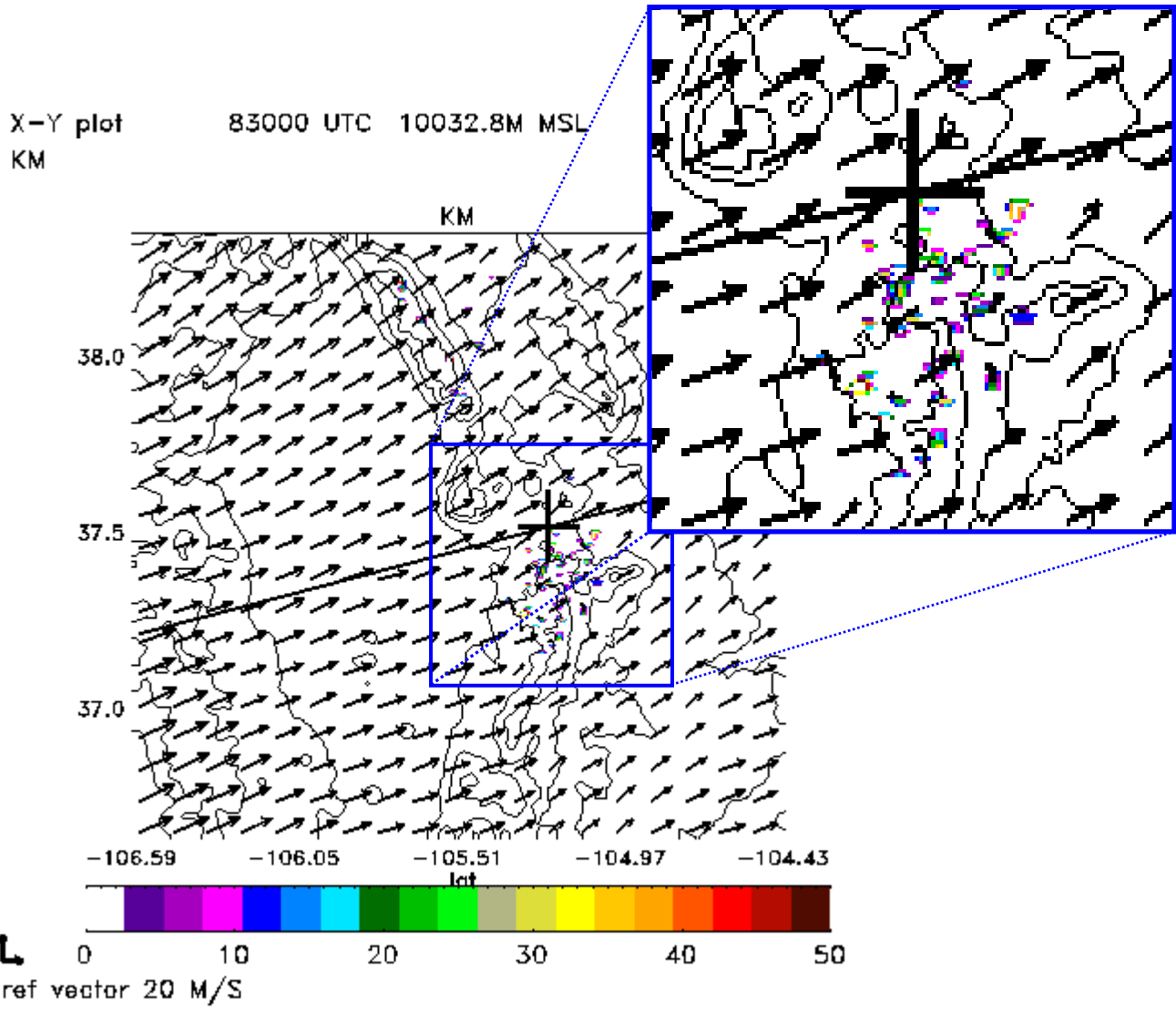


Fig. 11. As in Fig. 9, except color contours of the eddy dissipation rate, KM, which is proportional to the turbulent kinetic energy. Note the numerous small patches of KM scattered throughout the area corresponding to the decelerated flow in Fig. 9.